Differential multiple-quantum relaxation arising from cross-correlated time-modulation of isotropic chemical shifts

Karin Kloiber & Robert Konrat*
Institute of Organic Chemistry, University of Innsbruck, Innrain 52a, A6020 Innsbruck, Austria

Abstract

In this paper it is demonstrated that cross-correlated time modulation of isotropic chemical shifts ('conformational exchange') leads to differential relaxation of double- and zero-quantum coherences, respectively. Quantitative information can be obtained from the time dependence of the interconversion between the two two-spin coherences $2I_xS_x$ and $2I_yS_y$, induced by the differential relaxation. The effect is illustrated with an application to $^{13}C,^{15}N$-labeled quail CRP2(LIM2), by studying ^{15}N-$^1H^N$ multiple-quantum relaxation. Significant cross-correlated fluctuations of isotropic chemical shifts were observed for residues which are part of a disordered loop region connecting two β-strands in CRP2(LIM2). Differential $^1H^N$ and ^{15}N exchange contributions to multiple-quantum relaxation observed at these sites illustrate the complex interplay between hydrogen bonding events and conformational reorientations in proteins.

Introduction

NMR spectroscopy provides increasingly detailed descriptions of the structural dynamics of macromolecules in solution (Peng and Wagner, 1994; Dayie et al., 1996; Palmer et al., 1996; Daragan and Mayo, 1997). Most of the dynamic NMR studies relied on measurement of ^{15}N relaxation rates as a probe to sense protein dynamics. Unfortunately, using only a single site of the peptide planes does not cover all the dynamical features of the protein in solution. To overcome this limitation, NMR relaxation studies of the ^{13}CO nucleus have been performed (Zeng et al., 1996; Dayie et al., 1997; Engelke and Rüterjans, 1997; Fischer et al., 1998), although the quantitative interpretation of these relaxation rates remained difficult. Recently, cross-correlated relaxation has been shown to represent another valuable source of structural and dynamical information. NMR methods have been devised that measure cross-correlated fluctuations of

relaxation mechanisms, be it different dipolar couplings (DD) (Reif et al., 1997; Pelupessy et al., 1999) or dipolar couplings and chemical shift anisotropy (CSA) (Yang et al., 1997, 1998; Yang and Kay, 1998). Additionally, CSA-CSA cross correlations have been proposed (Vold and Vold, 1978; Werbelow, 1987; Konrat and Sterk, 1993; Kumar and Kumar, 1996) and experimentally demonstrated (Norwood et al., 1999; Pang et al., 1999; Pellecchia et al., 1999; Pervushin et al., 1999; Tessari and Vuister, 2000).

Local dynamic processes in proteins, however, are not confined to fast (picosecond–nanosecond) structural librations but can also comprise thermally activated motions on microsecond–millisecond time scales, which are often important for protein function (Fersht, 1985). These motional processes are probed by different experimental strategies. Firstly, by measuring the transverse relaxation rate R_2 using a Carr–Purcell–Meiboom–Gill (CPMG) sequence (Carr and Purcell, 1954; Meiboom and Gill, 1958) as a function of the CPMG delay (Gutowsky et al. 1965; Orekhov et al., 1994, 1995). Secondly, by measuring the spin-lock relaxation rate $R_{1\rho}$ as a function of the

radiofrequency spin-lock amplitude (Deverell et al., 1970; Peng and Wagner, 1992; Szyperski et al., 1993), where the effective field axis is preferably tilted by an angle θ relative to the static magnetic field axis (Desvaux et al., 1995; Akke and Palmer, 1996; Zinn-Justin et al., 1997; Akke et al., 1998; Mulder et al., 1998).

Here we show, both theoretically and experimentally, that the presence of ms-μs motional processes, which cause a modulation of the isotropic chemical shifts of two nuclei involved in multiple-quantum coherences, is manifested in differential relaxation of double- and zero-quantum coherences. During the preparation of the manuscript, the possibility of this exchange correlation phenomenon was independently mentioned by Tessari and Vuister (2000). As a first example, we discuss the differential relaxation of ^{15}N-^{1}H^{N} double- and zero-quantum coherences in the fully ^{13}C, ^{15}N-enriched (although ^{15}N-labeled protein samples are sufficient) carboxyl-terminal LIM domain CRP2(LIM2) of quail cysteine- and glycine-rich protein CRP2, a protein involved in cell growth and differentiation (Weiskirchen et al., 1995).

Materials and methods

Uniformly ^{13}C,^{15}N-labeled carboxyl-terminal LIM domain qCRP2(LIM2) of quail cysteine- and glycine-rich protein CRP2 was prepared and purified as described previously. Signal assignments and structural data of qCRP2(LIM2) have already been published (Konrat et al., 1997).

All NMR experiments were performed on a Varian UNITY Plus 500 MHz spectrometer equipped with a pulsed field gradient (PFG) unit using a triple resonance probe with actively shielded z gradients. The sample contained 1.5 mM of ^{13}C,^{15}N-labeled qCRP2(LIM2), as well as 20 mM potassium phosphate buffer pH 7.2, 50 mM KCl and 0.5 mM dithiothreitol in 90% H$_2$O/10% D$_2$O. All spectra were recorded at 26 °C. All experiments performed used spectral widths of 1650 × 8000 Hz in the t$_1$ × t$_2$ dimensions. The ^{1}H carrier was set to the frequency of the water resonance (4.76 ppm), and the ^{15}N carrier frequency was set to 119 ppm. Decoupling of ^{15}N spins during acquisition was performed using the WALTZ decoupling scheme (Shaka et al., 1983) with a decoupling power of $\gamma B_1 = 900$ Hz.

Differential ^{15}N-^{1}H^{N} DQ-ZQ-relaxation. The sequence for measuring the differential relaxation of ^{15}N-^{1}H^{N} double- and zero-quantum coherences derives from the conventional ^{15}N 2D-HSQC experiment (Figure 1). It comprises gradient selection combined with sensitivity enhancement (Cavanagh et al., 1991; Palmer et al., 1991; Kay et al., 1992b). The essential difference is that prior to the ^{15}N t$_1$ evolution period, a relaxation delay (T$_C$) is inserted during which ^{15}N-^{1}H^{N} multiple-quantum coherences evolve. The two ^{15}N and ^{1}H^{N} 90 °C pulses applied simultaneously at time point a of the sequence generate the coherence, 2N$_x$H$_x$, which is allowed to evolve between the time points a and b in the sequence (T$_C$).

The operator 2N$_x$H$_x$ can be decomposed into a sum of double- (DQ) and zero- (ZQ) quantum coherences

$$2N_xH_x = 0.5(N^+ + N^-)(H^+ + H^-) =$$
$$0.5(N^+H^+ + N^-H^+ + N^+H^- +$$
$$N^-H^-) \tag{1}$$

where I$^+$ and I$^-$ are raising and lowering operators ($I_\pm = I_x \pm iI_y$), respectively. The orthogonal component 2N$_y$H$_y$ is given by

$$2N_yH_y = -0.5(N^+ - N^-)(H^+ - H^-) =$$
$$-0.5(N^+H^+ - N^-H^+ - N^+H^- +$$
$$N^-H^-) \tag{2}$$

Evolution of double- and zero-quantum expectation values during the relaxation period T$_C$ (between time points a and b) proceeds as follows

$$< 2N_xH_x > (T_C) = 0.5 \exp\{-R_{DQ}T_C\}(< N^+H^+ > (0)$$
$$+ < N^-H^- > (0))$$
$$+ 0.5 \exp\{-R_{ZQ}T_C\}(< N^-H^+ > (0)$$
$$+ < N^+H^- > (0)) \tag{3}$$

and

$$< 2N_yH_y > (T_C) = -0.5 \exp\{-R_{DQ}T_C\}(< N^+H^+ > (0)$$
$$+ < N^-H^- > (0))$$
$$+ 0.5 \exp\{-R_{ZQ}T_C\}(< N^-H^+ > (0)$$
$$+ < N^+H^- > (0)) \tag{4}$$

Differential relaxation ($R_{DQ} \neq R_{ZQ}$, see Theory) of double- and zero-quantum coherences leads to a partial conversion of 2N$_x$H$_x$ into 2N$_y$H$_y$. With
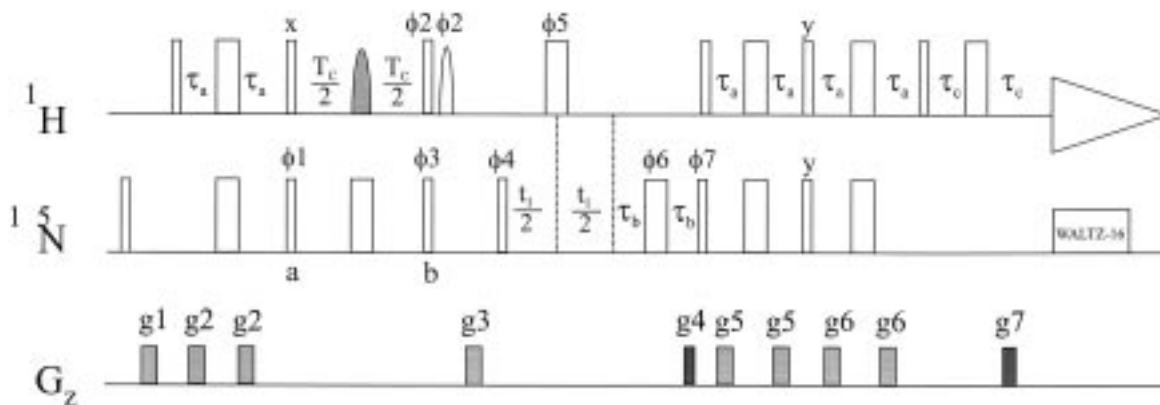
Figure 1. Pulse scheme for the measurement of differential ^{15}N-^{1}H^N multiple-quantum relaxation. Narrow and wide pulses indicate 90° and 180° pulses, respectively, and, unless indicated otherwise, all pulses are applied along the x-axis. The ^{1}H and ^{15}N carriers were positioned at 4.72 ppm (water) and 119 ppm. ^{15}N pulses use a 6 kHz field, with WALTZ (Shaka et al., 1983) decoupling achieved with a 1 kHz field. The water-selective ^{1}H 90° pulse (phase $\phi2$) is applied as a 2.2 ms rectangular pulse, with the carrier on the water resonance. Selective inversion (shaded pulse) of the amide protons in the middle of the relaxation period T_C is achieved using a RE-BURP inversion pulse (Geen and Freeman, 1991) (3.1 ms, 2.02 kHz peak radiofrequency (rf)). The ^{1}H carrier frequency is kept at the water resonance, and the ^{1}H^N selective inversion pulse is phase modulated so that the center of inversion is located at 8 ppm. Numerical simulations show that 95% inversion is achieved between 6.65–9.35 ppm. The values for τ_a, τ_b and τ_c were set to 2.25, 1.375 and 0.5 ms, respectively. The phase cycling was $\phi1$ = y,−y; $\phi2$ = y or x; $\phi3$ = y or x; $\phi4$ = x; $\phi5$ = x,−x; $\phi6$ = 2(x),2(y),2(−x),2(−y), $\phi7$ = x, and receiver was x,−x,−x,x. Two datasets are recorded in which the phases are either set to $\phi2$ = y;$\phi3$ = y (reference experiment) or $\phi2$ = x;$\phi3$ = x (differential multiple-quantum relaxation experiment). Quadrature detection in F_2 employs the enhanced sensitivity pulsed field gradient method (Kay et al., 1992; Schleucher et al., 1993) where for each value of t_1 separate data sets are recorded for (g7, $\phi7$) and (−g7, $\phi7$ +180°). For each successive t_1 value, $\phi4$ and the phase of the receiver are incremented by 180°. Gradient levels were as follows: g1 = 1.0 ms, 8 Gcm^{-1}; g2 = 0.5 ms, 8 Gcm^{-1}; g3 = 1 ms, 6 Gcm^{-1}; g4 = 1.25 ms, 30 Gcm^{-1}; g5 = 0.15 ms, 15 Gcm^{-1}; g6 = 0.15 ms, 15 Gcm^{-1}; and g7 = 0.125 ms, 29 Gcm^{-1}.

$\Delta R_{MQ} = R_{DQ} - R_{ZQ}$ (ΔR_{MQ} comprises possible relaxation contributions, i.e. CSA-CSA cross correlations, dipole–dipole cross correlations and contributions due to fluctuations of the isotropic chemical shift, see Theory), the ratio of the expectation values $<2N_yH_y>$ and $<2N_xH_x>$ is given by

$$< 2N_yH_y > / < 2N_xH_x > = (-\exp\{-R_{DQ}T_C\}$$
$$+ \exp\{-R_{ZQ}T_C\})/(\exp\{-R_{DQ}T_C\} + \exp\{-R_{ZQ}T_C\}) \quad (5)$$
$$= \tanh(\Delta R_{MQ}T_C/2)$$

In order to quantify ΔR_{MQ}, two sets of spectra are recorded differing only by the phases ($\phi2$ = y,x; $\phi3$ = y,x) of the two simultaneous 90° pulses (at time point b in the sequence of Figure 1). In the reference experiment ($\phi2$ = y; $\phi3$ = y) $2N_xH_x$ is selected, whereas in the differential relaxation experiment ($\phi2$ = x;$\phi3$ = x) the orthogonal component $2N_yH_y$ is recorded. Note that in order to restore the water signal, the water selective flip-back pulse (Grzesiek and Bax, 1993) is applied with phase $\phi2$. Although a single T_C value is sufficient for determination of ΔR_{MQ}, five experiments were performed varying the relaxation delay T_C using the following values: 10, 20, 30, 40 and 50 ms. All spectra were recorded as 64 × 512 complex matrices with 32 scans per complex

t_1 point for the reference experiment and 256 scans for the differential relaxation experiment, and a repetition delay between scans of 1 s was used in all experiments. Estimates for ^{1}H^N T_2's were obtained using a Hahn's echo based on the sequence of Figure 1 with identical parameters but without applying ^{15}N pulses between time points a and b in the sequence. Thus, ^{1}H antiphase magnetization, $2H_xN_z$, evolves during the time period T_C. The CPMG delay (T_C) was incremented as follows: 0, 10, 15, 20, 25, 30 and 40 ms, respectively. The obtained ^{1}H^N transverse relaxation rates were not corrected for ^{15}N longitudinal relaxation contributions and the effect of indirect scalar ($^3J_{HNH\alpha}$) coupling constants.

Data processing

NMR data were processed using the NMRPipe software (Delaglio et al., 1995). All spectra were linearly predicted in t_1, weighted with a phase-shifted sine bell in t_1 and t_2, and zero-filled in each dimension prior to Fourier transformation. Peak integration was performed using NMRPipe (Delaglio et al., 1995). The differences in relaxation rates were determined from the experimental data according to Equation 5.

Theory

In this section, the theoretical expression for the difference in the auto-relaxation rates between double- and zero-quantum coherences is given. In what follows we focus only on the effect of a time modulation of the isotropic chemical shifts of the two nuclei engaged in the multiple-quantum coherence. Other contributions stemming from correlated fluctuations between different CSA contributions and from dipole–dipole cross-correlation rates can be found in the literature, (Vold and Vold, 1978; Werbelow, 1987; Konrat and Sterk, 1993; Kumar and Kumar, 1996). We start from the general spin hamiltonian for a two-spin system *IS*

$$H(t) = H_{0I} + H_{0S} + H_1(t) \qquad (6)$$

where H_{0I} and H_{0S} are constant in time and contain the Zeeman terms for the two spins I and S, respectively. In case of an exchanging system this is given by

$$H_{0I} = \sum_i p_i \omega_{0Ii} I_z \qquad (7a)$$

$$H_{0S} = \sum_i p_i \omega_{0Si} S_z \qquad (7b)$$

where p_i denote the populations of the various conformers and the summation runs over the individual conformers (in the simplest case treated here, a two-site exchange process is assumed) and ω_{0Ti} is the resonance frequency of spin T at site i. For reasons of simplicity we neglect any scalar couplings.

The time-dependent hamiltonian $H_1(t)$ comprises the simultaneous modulation of the isotropic I-spin $\sigma_I(t)$ and S-spin $\sigma_S(t)$ chemical shifts and can be expressed as contractions of irreducible tensors of rank 1,

$$H_1(t) = \gamma_I \sigma_I(t) I_z B_0 + \gamma_S \sigma_S(t) S_z B_0 \qquad (8)$$

where B_0 describes the static magnetic field in the laboratory frame and γ_i is the gyromagnetic ratio of nucleus i; as usual it was assumed that $B_\pm = 0$.

The explicit influence of H_{0I} and H_{0S} can be removed by transforming the Liouville equation into a new reference frame (interaction frame) (Abragam, 1986) yielding

$$\begin{aligned} H_1^*(t) &= \exp\{i(H_{0I} + H_{0S})t\} \\ &\quad H_1(t) \exp\{-i(H_{0I} + H_{0S})t\} \end{aligned} \qquad (9)$$

The transformed Liouville equation is thus

$$d\sigma^*(t)/dt = -i[H_1^*(t), \sigma^*(t)] \qquad (10)$$

$\sigma^*(t)$ denotes the density operator in the new reference frame. Under conditions that have been described in detail (Abragam, 1986), the quantum-mechanical master equation in the interaction representation is

$$\frac{d\sigma^*}{dt} = -\frac{1}{2} \int\limits_{-\infty}^{\infty} \overline{[H_1^*(t), [H_1^*(t-\tau), (\sigma^* - \sigma_0^*)]]} d\tau \qquad (11)$$

Equation 11 can be converted into an operator equation by expressing the density operator in terms of basis operators. The exchange contribution R_{ex} to the auto-relaxation rate Γ_{rr} of the operator B_r ($B_r = I_z$, $I_\pm$, S_z, $S_\pm$, $I_\pm S_z$, $I_z S_\pm$, $I_\pm S_\pm$) is given by

$$
\begin{aligned}
R_{ex} = &-\frac{B_0^2}{2}\gamma_I\gamma_I < B_r|[I_z, [I_z, B_r]] > \int\limits_{-\infty}^{\infty} \overline{\sigma_I(t)\sigma_I(t-\tau)} d\tau \\
&-\frac{B_0^2}{2}\gamma_S\gamma_S < B_r|[S_z, [S_z, B_r]] > \int\limits_{-\infty}^{\infty} \overline{\sigma_S(t)\sigma_S(t-\tau)} d\tau \\
&-\frac{B_0^2}{2}\gamma_I\gamma_S < B_r|[I_z, [S_z, B_r]] > \int\limits_{-\infty}^{\infty} \overline{\sigma_I(t)\sigma_S(t-\tau)} d\tau \\
&-\frac{B_0^2}{2}\gamma_S\gamma_I < B_r|[S_z, [I_z, B_r]] > \int\limits_{-\infty}^{\infty} \overline{\sigma_S(t)\sigma_I(t-\tau)} d\tau
\end{aligned} \qquad (12)
$$

Due to the presence of exchange contributions to the relaxation of both spins, also cross terms between the two exchange contributions (i.e. $[I_z, [S_z, B_r]]$ and $[S_z, [I_z, B_r]]$) have to be considered. From Equation 12 it is apparent that exchange cross terms do not contribute to the relaxation of transverse one-spin order, since the double commutator vanishes in case of transverse magnetization from a single spin ($B_r = I_\pm$, $S_\pm$). The situation becomes entirely different if multiple-quantum coherences (transverse multi-spin order) are present. In this case the double-commutator does not vanish anymore and thus the exchange cross terms do contribute to the relaxation rate of the multi-spin order.

We concentrate on the contribution of these exchange cross terms to the relaxation of double-quantum ($B_r = I_+S_+$) and zero-quantum ($B_r = I_+S_-$) coherences in a two-spin system and consider the case where the two spins I and S are exchanging between two sites A and B, with p_A and p_B being the relative populations of the two sites, and $\tau_{ex} = p_B/k_1 = p_A/k_{-1}$ is the exchange lifetime. k_1 and k_{-1} are the forward and backward exchange rates, respectively. The ensemble average in Equation 12 is calculated using the solutions of the coupled differential equations describing the exchange process as given by Wennerström, 1972. Using the commutator relationship $[I_z, I_\pm] = \pm I_\pm$ one gets

$$\begin{aligned} R_{DQ} &= R_{DQ0} + \Delta\delta(I) + \Delta\delta(S) \\ &\quad + 2\Delta\omega(I)\Delta\omega(S)p_A p_B \tau_{ex} \end{aligned} \qquad (13a)$$
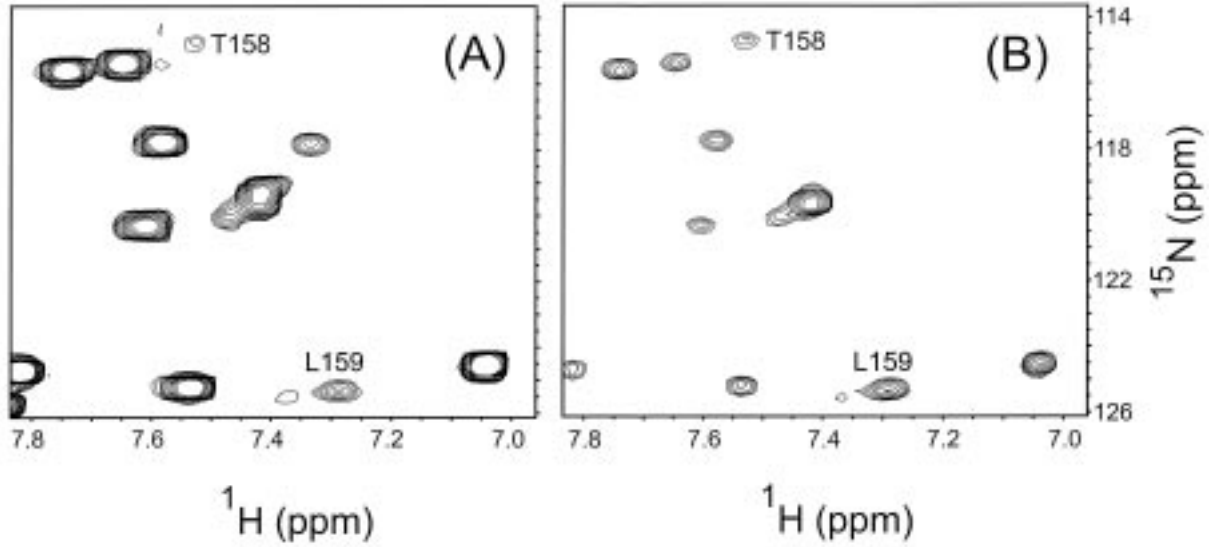
Figure 2. Zoom of 2D spectra of CRP2(LIM2) obtained with the sequence of Figure 1 of (A) the reference experiment and (B) the differential multiple-quantum relaxation experiment, using T_C = 30 ms. The total measuring time was 1.3 h (32 scans) for experiment A and 10.5 h (256 scans) for experiment B.

$$R_{ZQ} = R_{ZQ0} + \Delta\delta(I) + \Delta\delta(S)$$
$$-2\Delta\omega(I)\Delta\omega(S)p_A p_B \tau_{ex} \quad (13b)$$

where R_{DQ0} and R_{ZQ0} are the double- and zero-quantum auto-relaxation rates without chemical exchange. $\Delta\delta(I) = \Delta\omega(I)^2 p_A p_B \tau_{ex}$ and $\Delta\delta(S) = \Delta\omega(S)^2 p_A p_B \tau_{ex}$ are the exchange contributions to the transverse relaxation of spin I and S. $\Delta\omega(I)$ and $\Delta\omega(S)$ are the chemical shift differences $(\omega_A - \omega_B)$ [rad.s^{-1}] between the two sites for spins I and S, respectively. As can be seen from Equations 13a,b, the difference in the auto-relaxation rates of double- and zero-quantum coherences now also contains a contribution from correlated fluctuations of the isotropic chemical shifts of the two spins. The difference between the auto-relaxation rates R_{DQ0} and R_{ZQ0} is given by (Vold and Vold, 1978; Wokaun and Ernst, 1978; Werbelow, 1987; Konrat and Sterk, 1993; Kumar and Kumar, 1996):

$$R_{DQ0} - R_{ZQ0} = 2\Gamma_{I,S} + 2\eta_{IS,IS} + 2\sum_x \lambda_{IX,SX} \quad (14)$$

where the first term $\Gamma_{I,S}$ is the contribution from the cross correlation between the two CSA interactions, the second term $\eta_{IS,IS}$ originates from dipolar interactions giving rise to a heteronuclear NOE, and the third term comprises all possible dipole–dipole cross correlations $\lambda_{IX,SX}$ to other remote spins.

Results and discussion

Figure 1 illustrates the pulse scheme which was used to measure the differential relaxation of double- and zero-quantum coherences comprising the backbone amide nitrogens and protons of ^{13}C,^{15}N-labeled carboxyl-terminal LIM domain qCRP2(LIM2) from quail cysteine- and glycine-rich protein CRP2. Note that ^{13}C-labeling is not necessary for the performance of the experimental scheme in Figure 1. Two parts of the orthogonal datasets are shown in Figure 2. The good dispersion of the peaks in both frequency dimensions allowed for the quantification of differential multiple-quantum relaxation for 49 residues of CRP2(LIM2). Figure 3 shows ratios of intensities, $<2N_yN_y>/<2N_xN_x>$, as a function of T_C, for four different residues in CRP2(LIM2). As can be seen from the figure, the ratio agrees very well with the theoretical dependence of Equation 5. Although the replacement of the amide proton by a bulk water proton due to intermolecular exchange gives rise to a slight decrease of the measured cross-correlated exchange, no significant effects were observed for relaxation times smaller than 50 ms. However, if larger durations of T_C (i.e. T_C > 50 ms) are used, such effects become noticeable and lead to a deviation from Equation 5.

The experimentally determined relaxation rate difference, $\Delta R_{MQ} = R_{DQ} - R_{ZQ}$, varied between 0.58 s^{-1} (Ile166) and 35.7 s^{-1} (Leu159), with an

Table 1. Comparison between experimental $\Delta\delta_{MQ}$(exp.) and calculated $\Delta\delta_{MQ}$(calc.) cross-correlated exchange contributions to the differential multiple-quantum relaxation ΔR_{MQ}

Residue	$\Delta\delta_{MQ}$(exp.)[a] (s^{-1})	$\Delta\delta_{MQ}$(calc.)[b] (s^{-1})	$\Delta\delta$ (^{15}N)[c] (s^{-1})	$\Delta\delta$ (^{1}H^N)[d] (s^{-1})
Leu154	4.84	28.4	6.8	7.4
Thr158	30.74	32.2	**18.0**[e]	3.6
Leu159	32.74	52.1	4.7	**36.1**[e]

[a] $\Delta\delta_{MQ}$(exp.) was calculated from the difference between ΔR_{MQ}(i) $-$ ΔR_{MQ}(average). ΔR_{MQ}(average) was determined to 2.96 s^{-1}.

[b] $\Delta\delta_{MQ}$(calc.) was calculated based on Equations 13a, 13b, assuming a totally correlated two-state exchange model, $\Delta\delta_{MQ}$(calc.) $= 4(\Delta\delta(^{15}N))^{1/2} (\Delta\delta(^1H^N))^{1/2} = 4\Delta\omega(^{15}N)\Delta\omega(^1H^N)p_Ap_B\tau_{ex}$, and using the estimates for exchange contributions $\Delta\delta$ (^{15}N) and $\Delta\delta$ (^{1}H^N), respectively.

[c] Exchange contributions for ^{15}N, $\Delta\delta(^{15}N) = \Delta\omega^2(^{15}N)p_Ap_B\tau_{ex}$, were obtained from a model-free analysis (Lipari and Szabo, 1982a, 1982b) of ^{15}N relaxation data (Konrat et al., 1997).

[d] Exchange contributions for ^{1}H^N, $\Delta\delta$ (^{1}H^N) $= \Delta\omega^2(^1H^N)p_Ap_B\tau_{ex}$, were estimated from the differences between the individual $(1/T_2)$ (^{1}H^N)(i) and $(1/T_2)^0$ (^{1}H^N). $(1/T_2)^0$ (^{1}H^N) was assumed to be representative of an amide proton, which is conformationally rigid and slowly exchanging with bulk water. For $(1/T_2)^0$ (^{1}H^N), the ^{1}H^N of Trp140 (^{1}H^N-T$_2$: 72 ms) was used in the analysis. Trp140 is located in a well-defined β-strand and the amide proton shows high protection from intermolecular exchange with the solvent.

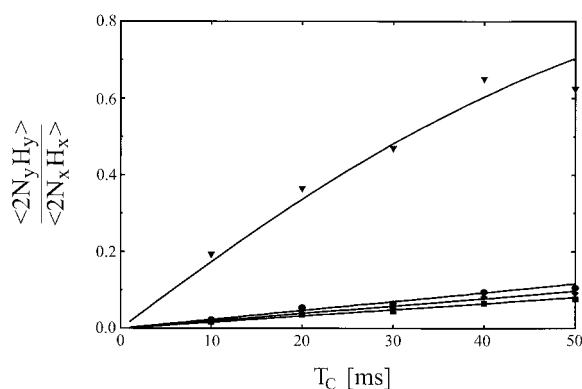[e] The dominating exchange contributions are given in bold.

Figure 3. Ratio of intensities, $<2N_yH_y>/<2N_xH_x>$, as a function of T_C, for four residues in CRP2(LIM2). The solid lines are drawn according to Equation 5. Filled triangle: Thr158; filled square: Ser121; filled diamond: Gly151; and filled circle: Cys123.

Figure 4. Differential multiple-quantum relaxation, ΔR_{MQ}, as a function of residue in CRP2(LIM2). Residues 154–159 are part of a conformationally flexible loop region connecting the two β-strands βVI (from residue Lys152 to residue Leu154) and βVII (from residue Thr160 to residue Lys162) in CRP2(LIM2) (Konrat et al., 1997). Insert: Residues with significantly increased ΔR_{MQ} values (Leu154, Thr158 and Leu159) are displayed on a ribbon representation of CRP2(LIM2). The picture was generated with the program MOLSCRIPT (Kraulis, 1991).

average value of 2.96 ± 1.26 s^{-1} (omitting residues Leu154, Thr158 and Leu159, which displayed significantly larger relaxation rate differences, see below). The precision limit of the obtained relaxation rate differences ΔR_{MQ} was derived from Monte Carlo simulations of the distributions of the experimental peak intensities. The root-mean-square baseline noises in the two experiments were taken as a measure of the standard deviations of the peak heights in these experiments. The average error was calculated to be 0.12 ± 0.1 s^{-1}. Figure 4 shows a residue plot of ΔR_{MQ} versus residue number. As was the case for cross correlations involving other nuclei of the pep-
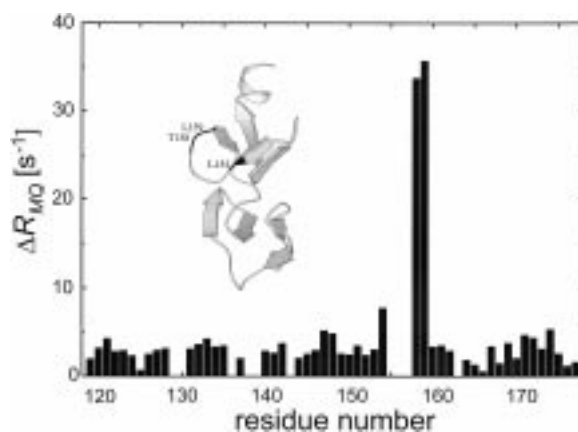
tide plane (Brutscher et al., 1998; Ghose et al., 1998), the values of ΔR_{MQ} are not uniform but instead show a significant variation. From Equation 14 it can be seen that there are various possible explanations for this difference. First, a variation of both the orientations and magnitudes of the ^{15}N and ^{1}H^N CSA tensors would modify the CSA/CSA cross correlation contribution. Secondly, dependent on the secondary

structure, the different dipole–dipole cross correlation terms in Equation 14 would change. Thirdly, the presence of internal dynamics also modifies the various average cross-correlation rates in Equation 14. Finally, motional anisotropy has to be considered, as it leads to a dependence of the various cross-correlated relaxation rates on the orientation of the participating interaction principal frames in the tensor of rotational diffusion. In order to delineate all the various contributions, more experiments have to be performed, which is, however, not the main thrust of the present investigation. Of particular interest and of major concern are the significantly increased values of ΔR_{MQ} for residues Leu154, Thr158, and Leu159. The ΔR_{MQ} for these residues were: Leu154: 7.8 s^{-1}; Thr158: 33.7 s^{-1} and Leu159: 35.7 s^{-1}. There is compelling evidence that these residues are located in a conformationally flexible loop region connecting two β-strands (Konrat et al., 1997). Other loop and turn regions in qCRP2(LIM2) show less pronounced conformational exchange processes. A model-free analysis of the ^{15}N relaxation data (obtained with a CPMG sequence; Konrat et al., 1997) revealed significant exchange contributions for these residues (Table 1). Additionally, the presence of conformational flexibility is evidenced by the fact that large deviations from average differential line broadening $\Delta R_{DQ/ZQ}$ of ^{13}C′(i−1)-^{15}N(i) multiple-quantum (MQ) coherences were also observed for ^{13}C′(i−1)-^{15}N(i) DQ/ZQ of residues Leu154, Thr158 and Leu159 in CRP2(LIM2). The values were obtained with a pulse sequence similar to the sequence proposed by Zuiderweg and co-workers (Pellecchia et al., 1999): ($\Delta R_{C',N}$: Leu154: −8.0 s^{-1}; Thr158: +19.3 s^{-1}; Leu159: +0.1 s^{-1}; average value: −2.5 ± 1.4 s^{-1}). The dramatic increase in ^{1}H^N-^{15}N DQ/ZQ relaxation differences, ΔR_{MQ}, for residues Leu154, Thr158 and Leu159 cannot be accounted for by realistic modifications of the ^{15}N and ^{1}H^N CSA tensors or the introduction of (fast) local anisotropic motion at these two sites. Finally, additional dipole-dipole cross-correlations to remote spins can also be ruled out. The only relaxation mechanism which can be responsible for this dramatically increased relaxation difference is a cross-correlated time modulation of the ^{15}N and the ^{1}H isotropic chemical shifts. To further corroborate our conclusion, we have compared experimental $\Delta\delta_{MQ}$(exp.) and calculated $\Delta\delta_{MQ}$(calc.) exchange contributions to ΔR_{MQ} (Table 1). Note that only the total exchange contributions ($\Delta\delta_{MQ}$, $\Delta\delta(^{15}$N), $\Delta\delta(^1$H^N)) to the transverse relaxation were considered. No attempts have been made to extract populations, frequency shifts or exchange lifetimes. The calculation serves to demonstrate that cross-correlated exchange is the only plausible relaxation mechanism to give rise to these significant differential line-broadening effects. From inspection of Table 1 it can be seen that the magnitudes of $\Delta\delta_{MQ}$(exp.) for Leu154, Thr158 and Leu159 are reasonably reproduced by taking into account cross-correlated fluctuations of the ^{1}H^N and ^{15}N isotropic chemical shifts. Of course, the accuracy of the estimated ^{1}H^N and ^{15}N exchange contributions limits the agreement between calculated and experimental exchange cross-correlation rates $\Delta\delta_{MQ}$ (Table 1). Secondly, the neglect of intermolecular exchange with bulk water leads to a slight overestimation of the calculated cross-correlated exchange rate $\Delta\delta_{MQ}$(calc.). Additionally, the derivation of the exchange contributions to the differential multiple-quantum relaxation (Equations 13a,13b) strictly assumes a totally correlated two-site exchange process. However, conformational reorientations in proteins can be significantly more complex and consequently require more elaborate motional models (e.g. correlated multi-site exchange).

It is interesting to note that the relative exchange contributions of ^{15}N and ^{1}H^N to ΔR_{MQ} of Leu154, Thr158 and Leu159 differ significantly. The exchange contributions to ΔR_{MQ} of both ^{15}N and ^{1}H^N for Leu154 are almost identical. For Thr158, differential multiple-quantum relaxation is mainly governed by ^{15}N contributions, whereas for Leu159 ΔR_{MQ} is dominated by contributions stemming from ^{1}H^N transverse relaxation. The difference is governed by the mechanistic details of the structural isomerization processes at these molecular sites. For example, reversible opening and closing of hydrogen bonds at these sites transiently forms open, unprotected conformational substates, which subsequently can undergo structural reorientations. The different ^{1}H^N and ^{15}N exchange contributions to differential ^{1}H^N-^{15}N multiple-quantum relaxation observed for these residues suggest that the nature of these transient high-energy fluctuations varies significantly along the backbone of this conformationally flexible loop region. Note that these residues also display a different degree of agreement between experimental $\Delta\delta_{MQ}$(exp.) and calculated $\Delta\delta_{MQ}$(calc.) exchange contributions to ΔR_{MQ}. For Thr158 the agreement is very good, whereas for Leu154 and Leu159 only poor agreement is observed. At present, the precise nature of the structural isomerization processes at these backbone sites is not yet clear. The data for Thr158 are

consistent with a two-site conformational exchange process. However, additional conformational fluctuations (e.g. reversible hydrogen bond formation and/or breakage) occurring on a faster (sub-microsecond) time-scale may exist. In contrast, residues Leu154 and Leu159 may exist in a conformational equilibrium between three or more distinct conformations with μs-ms exchange lifetimes for the interconverting conformational substates. Interestingly, the qualitatively different conformational exchange behavior at these sites is also paralleled by different levels of amide protection from exchange with bulk water. The protection from exchange is considerably higher for Leu154 and Leu159 compared to Thr158. It thus seems plausible that the relative weakness of the hydrogen bond(s) at the site of Thr158 increases the rate constants of the reorientational processes preceding the subsequent local two-site exchange.

Somewhat smaller but still significantly larger than average ΔR_{MQ} values are found for residues Cys147, Ala148 and Lys174. Residues Cys147 and Ala148 are part of the rubredoxin-knuckle ('Rd-knuckle') (Konrat et al., 1997) of the second CCCC zinc-binding site in CRP2(LIM2). The conformation of this local structure element is partially stabilized by hydrogen bonding between backbone amide protons and thiolates of the zinc coordinating cysteine residues (Perez-Alvarado et al., 1994; Konrat et al., 1997). Whereas Cys147 exhibits slightly smaller than average T_2 values, there is no indication for conformational exchange processes for Ala148. Thus, it cannot be ruled out that the increase in ΔR_{MQ} values for Ala148 may be due to variations of the ^{15}N and ^{1}H^N CSA tensors (i.e. due to hydrogen bonding). Interestingly, the amide proton H^N of Ala148 (strand βV) forms a hydrogen bond to the carbonyl oxygen of Ile166 (strand βVIII), which additionally stabilizes the β-sheet arrangement in CRP2(LIM2) (Konrat et al., 1997). Lys174 terminates the C-terminal helix in CRP2(LIM2) and we suggest that a conformational exchange process reminiscent of helical fraying is responsible for this increased ΔR_{MQ} value.

Conclusions

We have demonstrated that a cross-correlated time-modulation of the isotropic chemical shifts of a spin pair incorporated in multiple-quantum coherences leads to a differential relaxation of double- and zero-quantum coherences, respectively. This differential relaxation effect is manifested in a partial conversion of the two-spin coherence term $2N_xH_x$ into $2N_yH_y$, which can be conveniently measured by simply adjusting the phases of two 90° ^{15}N and ^{1}H pulses, thereby selecting one of the two two-spin coherences. The difference in the multiple-quantum relaxation rates can be obtained from the intensity ratio of the two experiments. The effect can be understood using time-dependent perturbation theory by introducing a time-dependent Zeeman hamiltonian for the two spins in the multiple-quantum coherence.

Differential relaxation of double- and zero-quantum coherences provides valuable information about chemical shielding tensors and defines another valuable source of dynamic information. However, care has to be taken as far as the quantitative interpretation is concerned. For example, in a recent study Zuiderweg and co-workers (Pellecchia et al., 1999) have obtained CSA-CSA cross-correlation rates with high precision for the protein binase (12.3 kDa). They observed significant discrepancies between local protein dynamics for the C-terminus of the protein deduced either from CSA-CSA cross correlations $\Gamma_{N,C'}$ or from dipole–dipole cross-correlated relaxation rates $\Gamma_{NH,C'H}$. As this part of the protein comprises the active site of the enzyme, for which also extensive millisecond dynamics were observed (Pellecchia et al., 1999), it might be anticipated that the observed discrepancy may be due to cross-correlated time-modulation of the isotropic chemical shifts of the amide nitrogen and the carbonyl carbon, respectively.

In sum, we have demonstrated that cross-correlated chemical shift modulation provides an efficient relaxation mechanism for multiple-quantum coherences and can be used to monitor μs–ms protein structural fluctuations. This opens up new experimental means for the investigation of dynamic events in solution. Specifically, we anticipate that by a combined interpretation of single-quantum autorelaxation (Akke and Palmer, 1996; Mulder et al., 1998) (preferably at multiple magnetic field strengths) and differential multiple-quantum relaxation, exquisite information about the mechanistic details of conformationally exchanging spin systems (i.e. extent of correlated fluctuations, identification of multi-site exchange processes) will be obtained. Another possible application lies in the study of enzyme–ligand systems, where the number of structurally relevant intramolecular ligand NOEs is often scarce. In this case, the chemical shift modulation upon reversible ligand binding, when combined with quantum mechanical

shift calculations, may provide important structural information about the ligand conformation in the bound state and might be a valuable addition to other recently developed experiments based on cross-correlated relaxation (Blommers et al., 1999; Carlomagno et al., 1999). Moreover, the differential line broadening observed in multiple-quantum coherences may also be exploited in a way similar to the TROSY principle (Pervushin et al., 1998), which would allow for interesting applications in chemically exchanging (and rapidly decaying) spin systems. Finally, provided that multiple-quantum coherences can be established between remote spins separated by many residues in the primary sequence, one can envisage fascinating applications to study correlated and functionally important long-range ms–μs motions in enzymes.

Acknowledgements

References

Abragam, A. (1986) *The Principles of Nuclear Magnetism*, Clarendon Press, Oxford, U.K.

Akke, M. and Palmer, A.G. (1996) *J. Am. Chem. Soc.*, **118**, 911–912.

Akke, M., Liu, J., Cavanagh, J., Erickson, H.P. and Palmer III, A.G. (1998) *Nat. Struct. Biol.*, **5**, 55–59.

Blommers, M.L.J., Stark, W., Jones, C.E., Head, D., Owen, C.E. and Jahnke, W. (1999) *J. Am. Chem. Soc.*, **121**, 1949–1953.

Bremi, T. and Brüschweiler, R. (1997) *J. Am. Chem. Soc.*, **119**, 6672–6673.

Brutscher, B., Skrynnikov, N.R., Bremi, T., Brüschweiler, R. and Ernst, R.R. (1998) *J. Magn. Reson.*, **130**, 346–351.

Carlomagno, T., Felli, I.C., Czech, M., Fischer, R., Sprinzl, M. and Griesinger, C. (1999) *J. Am. Chem. Soc.*, **121**, 1945–1948.

Carr, H.Y. and Purcell, E.M. (1954) *Phys. Rev.*, **94**, 630–638.

Daragan, V.A. and Mayo, K.H. (1997) *Prog. NMR Spectrosc.*, **31**, 63–105.

Delaglio, F., Grzesiek, S., Vuister, G.W., Zhu, G., Pfeifer, J. and Bax, A. (1995) *J. Biomol. NMR*, **6**, 277–293.

Desvaux, H., Birlirakis, N., Wary, C. and Berthault, P. (1995) *Mol. Phys.*, **86**, 1059–1073.

Deverell, C., Morgan, R.E. and Strange, J.H. (1970) *Mol. Phys.*, **18**, 553–559.

Engelke, J. and Rüterjans, H. (1997) *J. Biomol. NMR*, **9**, 63–78.

Fersht, A. (1985) In *Enzyme Structure and Mechanism*, W.H. Freeman and Company, New York, NY, USA.

Fischer, M.W.F., Zeng, L., Pang, Y., Hu, W., Majumdar, A. and Zuiderweg, E.R.P. (1997) *J. Am. Chem. Soc.*, **119**, 12629–12642.

Fischer, M.W.F., Majumdar, A. and Zuiderweg, E.R.P. (1998) *Prog. NMR. Spectrosc.*, **33**, 207–272.

Garrett, D.S., Powers, P., Gronenborn, A.M. and Clore, G.M. (1991) *J. Magn. Reson.*, **95**, 214–220.

Geen, H. and Freeman, R. (1991) *J. Magn. Reson.*, **93**, 93–141.

Ghose, R., Huang, K. and Prestegard, J.H. (1998) *J. Magn. Reson.*, **135**, 487–499.

Grzesiek, S. and Bax, A. (1993) *J. Am. Chem. Soc.*, **115**, 12593–12594.

Gutowsky, H.S., Vold, R.L. and Wells, E.J. (1965) *J. Chem. Phys.*, **43**, 4107–4125.

Kay, L.E., Keifer, P. and Saarinen, T. (1992) *J. Am. Chem. Soc.*, **114**, 10663–10665.

Konrat, R. and Sterk, H. (1993) *Chem. Phys. Lett.*, **203**, 75–81.

Konrat, R., Weiskirchen, R., Kräutler, B. and Bister, K. (1997) *J. Biol. Chem.*, **272**, 12001–12007.

Kraulis, P.J. (1991) *J. Appl. Crystallogr.*, **24**, 946–950.

Kumar, P. and Kumar, A. (1996) *J. Magn. Reson.*, **A119**, 29–37.

Lipari, G. and Szabo, A. (1982a) *J. Am. Chem. Soc.*, **104**, 4546–4559.

Lipari, G. and Szabo, A. (1982b) *J. Am. Chem. Soc.*, **104**, 4559–4570.

Marion, D., Ikura, M., Tschudin, R. and Bax, A. (1989) *J. Magn. Reson.*, **85**, 393–399.

Meiboom, S. and Gill, D. (1958) *Rev. Sci. Instrum.*, **29**, 688–691.

Mulder, F.A.A., de Graaf, R.A., Kaptein, R. and Boelens, R. (1998) *J. Magn. Reson.*, **131**, 351–357.

Norwood, T.J., Tillett, M.L. and Lian, L.Y. (1999) *Chem. Phys. Lett.*, **300**, 429–434.

Orekhov, V.Y., Pervushin, K. and Arseniev, A.S. (1994) *Eur. J. Biochem.*, **219**, 887–896.

Orekhov, V.Y., Pervushin, K.V., Korzhnev, D.M. and Arseniev, A.S. (1995) *J. Biomol. NMR*, **6**, 113–122.

Pang, Y., Wang, L., Pellecchia, M., Kurochkin, A.V. and Zuiderweg, E.R.P. (1999) *J. Biomol. NMR*, **14**, 297–306.

Pellecchia, M., Pang, Y., Wang, L., Kurochkin, A.V., Kumar, A. and Zuiderweg, E.R.P. (1999) *J. Am. Chem. Soc.*, **121**, 9165–9170.

Pelupessy, P., Chiarparin, E., Ghose, R. and Bodenhausen, G. (1999) *J. Biomol. NMR*, **14**, 277–280.

Peng, J.W. and Wagner, G. (1992) *J. Magn. Reson.*, **98**, 308–332.

Pérez-Alvarado, G.C., Miles, C., Michelsen, J.W., Louis, H.A., Winge, D.R., Beckerle, M.C. and Summers, M.F. (1994). *Nat. Struct. Biol.*, **1**, 388–398.

Pervushin, K., Rieck, R., Wider, G. and Wüthrich, K. (1998) *Proc. Natl. Acad. Sci USA*, **94**, 12366–12371.

Reif, B., Hennig, M. and Griesinger, C. (1997) *Science*, **276**, 1230–1233.

Schleucher, J., Sattler, M. and Griesinger, C. (1993) *Angew. Chem. Int. Ed. Engl.*, **32**, 1489–1491.

Shaka, A.J., Keeler, J., Frenkiel, T. and Freeman, R. (1983) *J. Magn. Reson.*, **52**, 335–338.

Szyperski, T., Luginbühl, P., Otting, G., Güntert, P. and Wüthrich, K. (1993) *J. Biomol. NMR*, **3**, 151–164.

Tessari, M. and Vuister, G.W. (2000) *J. Biomol. NMR*, **16**, 171–174.

Vold, R.L. and Vold, R.R. (1978) *Prog. NMR Spectrosc.*, **12**, 79–133.

Weiskirchen, R., Pino, J.D., Macalma, T., Bister, K. and Beckerle, M.C. (1995) *J. Biol. Chem.*, **270**, 28946–28954.

Wennerström, H. (1972) *Mol. Phys.*, **24**, 69–80.

Wokaun, A. and Ernst, R.R. (1978) *Mol. Phys.*, **36**, 317–341.

Yang, D., Konrat, R. and Kay, L.E. (1997) *J. Am. Chem. Soc.*, **119**, 11938–11940.

Yang, D. Gardner, K.H. and Kay, L.E. (1998) *J. Biomol. NMR*, **11**, 213–220.

Yang, D. and Kay, L.E. (1998) *J. Am. Chem. Soc.*, **120**, 9880–9887.

Zeng, L., Fischer, M.W.F. and Zuiderweg, E.R.P. (1996) *J. Biomol. NMR*, **7**, 157–162.

Zinn-Justin, S., Berthault, P., Guenneugues, M. and Desvaux, H. (1997) *J. Biomol. NMR*, **10**, 363–372.